OPTIMISING OF A LOW-NOISE NEAR-CONCENTRIC CAVITY

by

CHAN JUN JIE

A THESIS SUBMITTED FOR THE DEGREE OF

B.SC. (HONS)

in

PHYSICS

in the

UNDERGRADUATE DIVISION

of the

NATIONAL UNIVERSITY OF SINGAPORE

2025

Supervisor:
Professor CHRISTIAN KURTSIEFER

Declaration

I hereby declare that this thesis is my original work and it has been written by me in its entirety. I have duly acknowledged all the sources of information which have been used in the thesis.

This thesis has also not been submitted for any degree in any university previously.

Chan Jun Jie

7 April 2025

Acknowledgments

Firstly, I would like to thank Professor Christian Kurtsiefer for the opportunity for me to join his lab even though I do not have any first-hand experience in an actual laboratory. Thank you for your guidance and support throughout my FYP journey

Next, I would like to thank Wen Xin for letting me be a part of his project. Thank you for taking time out to teach me the ways of the cavity. I appreciate your patience and effort in being my mentor in the field of cavities and my guide into the near-planar and near-concentric regime. You have been a great help in my journey of cavity enlightenment.

To the people in #01-04, thank you for being warm and welcoming. To Chang Hoong and Boon Long, I am greatly appreciative of you guys welcoming me into #01-04. It was a shame that I was not able to interact with you guys a lot, but nonetheless, I wish you guys good luck in your future endeavours and hope to see you guys now and again. Many thanks to Zifang for being the first familiar face in the lab and for all the delicious snacks. Thanks for your guidance and advice, and I hope that we can partake in more karting sessions.

Thank you to my batch mates for being with me throughout my 4 years in NUS. It has been an exciting and wonderful 4 years with you guys. All the inside jokes and fun times really tickled my Wronskian. To my volleyball mates in Recre, thank you for all the fun games. I can't wait to play with you guys again.

Lastly, to my family, for whom I am deeply grateful for, thank you for being so supportive and understanding throughout my whole academic life. And to Crystal, mi media naranja, thank you for being as supportive as you are, I am grateful for all our joyous memories together.

Contents

Abstract

OPTIMISING OF A LOW-NOISE NEAR-CONCENTRIC CAVITY

by

Chan Jun Jie

B.SC. (HONS) in PHYSICS

National University of Singapore

This thesis explores the use of Grade V titanium springs to increase the stability of a near-concentric cavity for use in atom-light experiments. Previous works attained passive sub-Angstrom stability with stainless steel springs, but traces of ferromagnetic elements caused the stability to be destroyed in the presence of magnetic field. We present our work as an alternative to stainless steel springs and further explored different spring parameters to optimise the sub-Angstrom passive stability. A passive length fluctuation of 0.092(3)Å was achieved with the new springs, a four-fold improvement over previous revisions.

List of Figures

List of Tables

Chapter 1

Introduction

Quantum mechanics emerged in the early twentieth century as a response to phenomena that classical physics could not explain, such as blackbody radiation and the photoelectric effect. In 1900, Max Planck introduced the idea of energy quantization, proposing that energy is emitted or absorbed in discrete units called quanta. This was the start of the quantum revolution. Today, quantum mechanics is the cornerstone of modern physics, with fields like quantum optics, solid-state physics, and atomic physics built entirely from quantum principles. In this thesis, we will delve into more detail regarding the subject of optical cavities.

Optical cavities have a variety of uses, such as in producing ultrastable lasers[1], gravitational wave detection [2], optical communication[3], and quantum networks[4] and are also heavily used in atomic physics as well. A simple example of a use case in atomic physics would be an atom sitting inside a simple two-plane mirror setup, a Fabry Perot resonator. This setup is greatly studied and forms the basis in the study of Cavity Quantum-Electrodynamics (CQED) κ is defined as the cavity loss

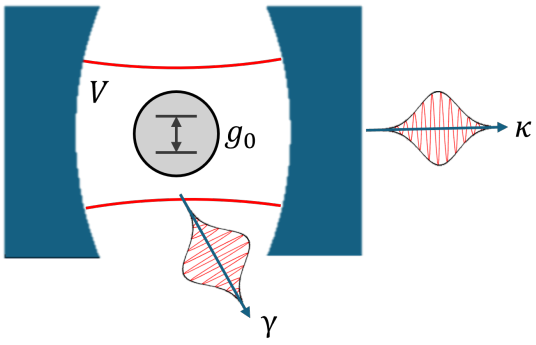

Figure 1.1: Simplified dissipative CQED model

rate and represents how quickly a photon is lost from the cavity. γ represents the atomic decay and describes the spontaneous emission rate of the atom. g_0 is the coupling strength of the atom and cavity, and a weak coupling can be thought of as $g_0 \ll (\gamma, \kappa)$ (i.e. losses in the system are greater than the coupling between photon and atom) and vice versa. As a result, the conditions for weak or strong coupling can be defined as a cooperativity factor,

$$C = \frac{g_0^2}{2\gamma\kappa} \tag{1.1}$$

The cooperativity factor, C describes the ratio between the coupling rate and the rate of losses. With this, we can define a weak coupling regime when $C > 1$ and a strong coupling regime when $C < 1$.

Notably, γ is fixed depending on your choice of atom, but g_0 and κ depend on cavity design and mirror reflectivity. Higher mirror reflectivity and longer cavities can lower the rate of photons lost due to mirror transmission, which in turn lowers κ. Using a mirror configuration that focuses the cavity field to a smaller volume (i.e. smaller mode volume, V) would result in increased g_0.

Many cavity configurations have been played with, such as microcavities [5], photonic crystal cavities and related integrated optical structures [6]. These designs use small-scale resonators (around μm scale) to minimise the mode volume, V. However, it was realised that a near-concentric cavity configuration could also achieve a similarly small mode volume, even with a cavity in the mm scale. However, as near-concentric cavities are prone to transverse misalignment. In this thesis, we will explore the use of springs on the passive length stability for use on a near-concentric cavity.

1.1 Relation to previous works

Typical optical cavities that use a 2-mirror Farby-Perot setup generally use near-planar configurations, where the radii of curvatures of the mirrors are much greater than the length of the mirror, as they are easier to align. To achieve a high cooperativity factor, higher reflectivity mirrors are used to reduce cavity loss rate κ and smaller-scale cavities to decrease modal volume. However, there is an alternative

configuration that allows for increased cooperativity compared to near-planar setups, even with mirrors of similar reflectivity,

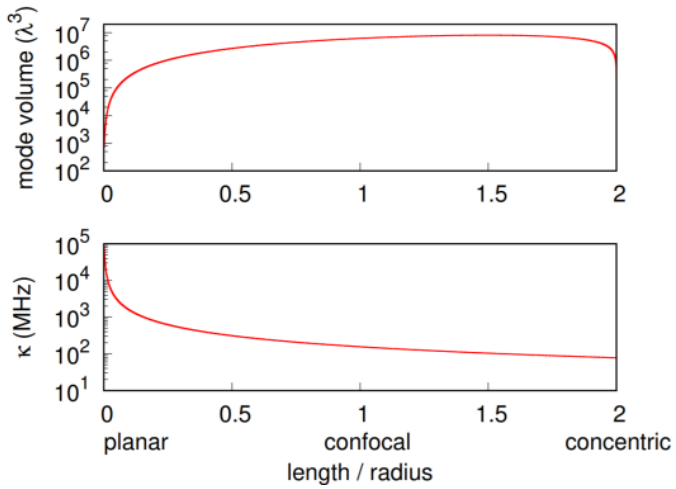

Figure 1.2: Plots of mode volume and cavity loss rate κ against cavity length to mirror radius. Notice that the mode volume of a near-planar is much smaller than a near-concentric, but κ is smaller for a near-concentric

In a previous work [7], it was realised that a near-concentric configuration could attain high coupling strength due to the nature of its geometry, allowing it to carry out atom-light experiments even with lower finesse than a near-planar configuration. They reasoned that this configuration could serve as an alternative to near-planar cavities, which require high reflectivity mirrors to minimise κ. However, it was shown that the near-concentric configuration is highly sensitive to transverse misalignments; 100 nm of transverse misalignment resulted in a total loss in transmission.

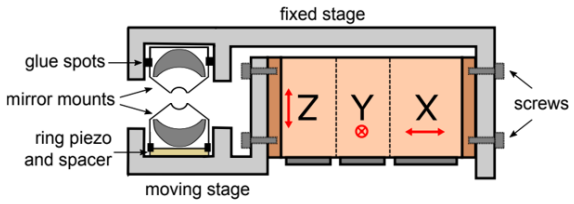

Figure 1.3: Cavity Design for Iteration 1

For the first revision of designs of near-concentric cavities [8], they glued three piezoelectric stack actuators together to correct the mirrors in 3-dimensional space. These actuators have a nominal range of ± 5 μm, but this range was not sufficient to correct for misalignments that occur during a baking cycle of around 5 μm.

In the second iteration [8], they use a flexural-based translation stage to provide a larger 3-dimensional translational movement range, up to 50×50×24 μm. However, due to the large movement range and mechanical complexity of the translation stage, the mechanical noise experienced by this setup was 5 times higher than the first iteration. It was also noted that the resonance frequency of the translation stage is typically less than 1 kHz.

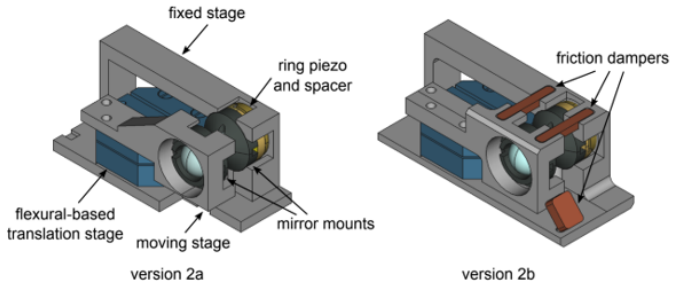

Figure 1.4: Cavity Design for Iteration 2

The third iteration [9] sought to solve the problems faced in the previous two iterations, such as insufficient actuator movement range, high mechanical noise, and low resonance frequency. The third cavity redesign aimed to be less bulky and mechanically complex than the previous two, looking to be as compact as possible. The design utilises three piezoelectric actuators with a nominal range of ±15 μm, which boasts a tip-tilt mechanism via the independent movement of each actuator.

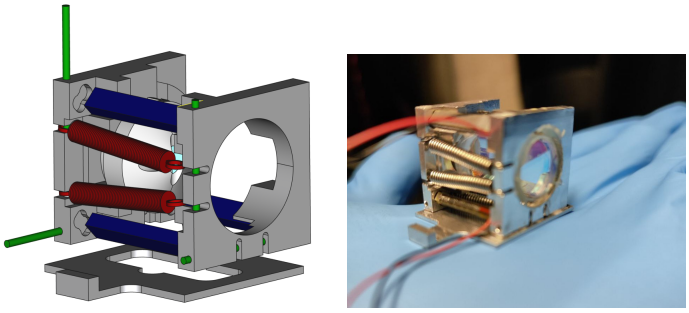

(a) CAD model of new cavity design

(b) Picture of assembled cavity

Figure 1.5: New iteration of cavity

One issue with the third design was its use of supposedly austenitic stainless steel springs. The springs would vibrate uncontrollably upon removal from a magnetic field. This would prove to be detrimental in atomic experiments where a magnetic

field is often used to trap atoms. Hence, the springs would have to be replaced with non-ferromagnetic materials.

1.2 Goal of Thesis

For a cavity of finesse, $\mathcal{F} \sim 600$ and to hit a noise factor $< 5\%$, our calculations indicate that a sub-Angstrom passive length fluctuation of 0.325Å has to be achieved. In this paper, we will focus on the usage of a different material for springs and the effects of different spring parameters on the cavity's passive length fluctuation.

1.3 Thesis Synopsis

The rest of this thesis is organized as follows. In Chapter 2, we will go through a brief review of optical cavities. We will discuss the sources and effects of noise on our cavity in Chapter 3 and how we are able to conduct noise measurements. Afterwards, in Chapter 4, we will explore how springs can be used to help improve the stability of a cavity. Chapter 5 follows by showing the results obtained from noise measurements to determine the cavity stability. We conclude the entire thesis as well as discuss further directions for future research in Chapter 6.

Chapter 2

Optical Cavity

As we start discussing optical cavities and their stability, it is important to first begin with the physics behind optical cavities. We will first go through the basics of optical cavities before going deeper into the dynamics and different cavity configurations.

2.1 Theory of Optical Cavity

A Fabry-Perot resonator is a simple optical cavity, which can be formed by placing 2 mirrors facing each other with distance L, When a photon enters the cavity, it will bounce between the two mirrors and undergo several round trips inside the resonator. The photon picks up a phase of $e^{-2i\frac{2\pi nL}{\lambda}} = e^{-2\phi}$ every round trip (refractive index n taken to be 1). If we take the reflectivity r and transmissivity t of the mirrors to be the same, the transmitted electric field can be derived,

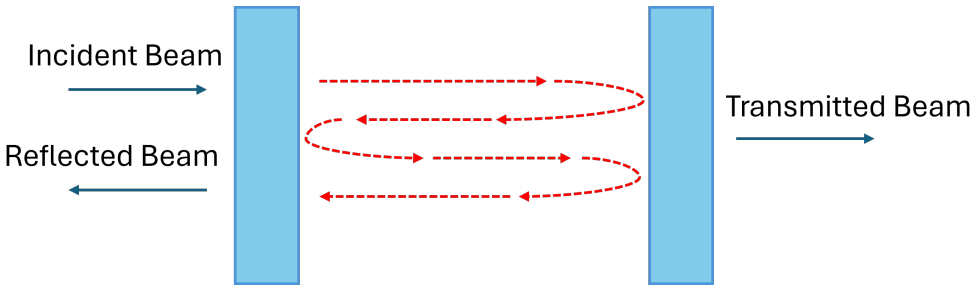

Figure 2.1: Simple Fabry Perot resonator

$$\begin{aligned} E_{trans} &= E_0|t|^2e^{-i\phi}\left(1+|r|^2e^{-2i\phi}+|r|^4e^{-4i\phi}+\dots\right) \\ &= \frac{E_0Te^{-i\phi}}{1-Re^{-2i\phi}} \end{aligned} \tag{2.1}$$

where $|t|^2$, $|r|^2$ are T and R respectively, and $T+R=1$. Similarly, the reflected electric field can also be derived in similar fashion, however, the first term does not pick up a π phase as the photon reflects from an optically less dense medium than the one it is travelling in. The resultant E_{reflec} is,

$$\begin{aligned} E_{reflec} &= E_0r\left(-1+|t|^2e^{2i\phi}+|t|^2|r|^2e^{4i\phi}+|t|^2|r|^4e^{6i\phi}+\dots\right) \\ &= E_0r(-1+\frac{Te^{2i\phi}}{1-Re^{2i\phi}}) \\ &= \frac{E_0r\left(e^{2i\phi}-1\right)}{1-Re^{2i\phi}} \end{aligned} \tag{2.2}$$

The transfer function, which is the ratio between the field and the incident field, for both the transmission and reflection from the cavity are,

$$\begin{aligned} \mathcal{T} &= \frac{Te^{-i\phi}}{1-Re^{-2i\phi}} \\ \mathcal{R} &= \frac{r\left(e^{2i\phi}-1\right)}{1-Re^{2i\phi}} \end{aligned} \tag{2.3}$$

The transfer functions are, however, not too useful for experiments, and it would be more useful to consider the intensity, I, of the field instead. Since $I \propto |E|^2$, the square of the transfer functions would give us the ratio between transmitted and reflected intensities, and the incident intensity. For this thesis, we only consider the square of the transmitted transfer function, $\mathcal{T}$,

$$\begin{aligned} |\mathcal{T}|^2 &= \frac{I_{trans}}{I_0} \\ &= \frac{T^2}{(1-R)^2+4R\sin^2(\phi)} \\ &= \frac{1}{1+\left(\frac{2\mathcal{F}}{\pi}\sin(\phi)\right)^2} \end{aligned} \tag{2.4}$$

where the finesse of the cavity, $\mathcal{F}$ is defined to be,

$$\mathcal{F} = \frac{\pi\sqrt{R}}{1-R} \tag{2.5}$$

From Equation 2.5, we can get a physical understanding of the finesse $\mathcal{F}$; finesse increases with the reflectivity of the mirrors. Using the transmission intensity ratio,$|\mathcal{T}|^2$, we are able to gather a few more cavity parameters. $|\mathcal{T}|^2$ is at maximum when ϕ is an integer π value; hence, ϕ can be rewritten to represent the cavity resonant frequency with respect to the cavity length.

$$\begin{aligned} \phi &= \frac{2\pi L}{\lambda} \\ \nu_{res} &= \frac{m\pi c}{2\pi L} \\ \nu_{res} &= \frac{mc}{2L} \end{aligned} \tag{2.6}$$

The spacing between resonant frequencies, ν_{res} is defined to be the free spectral range (FSR) for frequency,

$$\nu_{fsr} = \frac{c}{2L} \tag{2.7}$$

The FSR for length is also helpful as it will be used to convert frequency fluctuations to length fluctuations. For resonance in an optical cavity, integer multiples of half wavelengths will be equal to the length of the cavity (i.e. the wave will be standing in the cavity). As such, the free spectral length is defined to be,

$$L_{fsr} = \frac{\lambda}{2} \tag{2.8}$$

It can also be found that the linewidth of the optical cavity, $\delta\nu$ can be approximated to a ratio of Frequency FSR and finesse of the cavity, for$F \gg 1$,

$$\delta\nu \approx \frac{\nu_{fsr}}{\mathcal{F}} \tag{2.9}$$

2.2 CQED: Jaynes-Cummings model

CQED is the study of the interactions between atoms, or other particles, and light confined in a cavity. The Jaynes-Cummings (JC) model describes an ideal two-level atom system interacting with a single quantised mode of the optical cavity with no losses. The Hamiltonian of such a two-level system can be written as,

$$\begin{aligned} H &= H_{cavity} + H_{atom} + H_{int} \\ H &= \hbar\omega_c \hat{a}^\dagger \hat{a} + \hbar\omega_a \sigma_+ \sigma_- + \hbar g \left(a + a^\dagger\right)(\sigma_+ + \sigma_-) \end{aligned} \tag{2.10}$$

where ω_c and ω_a represent the resonant frequencies of the cavity and atom respectively, and g represents the atom-cavity interaction strength. Meanwhile, $a^\dagger$ and a represent the creation and annihilation operators for the cavity field, and $\sigma_+ = |g\rangle\langle e|$, $\sigma_- = |e\rangle\langle g|$ represent the raising and lowering operators between the ground and excited states (i.e. $|g\rangle$ and $|e\rangle$) of the atom. By applying the rotating-wave approximation (RWA), the Hamiltonian can be simplified to,

$$H = \hbar\omega_c \hat{a}^\dagger \hat{a} + \hbar\omega_a \sigma_+ \sigma_- + \hbar g \left(a\sigma_+ + a^\dagger \sigma_-\right) \tag{2.11}$$

g is defined to be

$$g = \sqrt{\frac{\omega_c}{2\epsilon_0 \hbar V}}\, d_{eg} \tag{2.12}$$

where V is the modal volume of the cavity, and d_{eg} is the dipole moment associated with the transition between $|g\rangle \rightarrow |e\rangle$. The g factor can be thought of as the rate of exchange of excitation between the atom and the electric field, built up by a photon with resonant frequency, ω_c.

2.2.1 Damped Cavity

The JC model assumes an ideal system without any losses. However, in practice, a cavity system would experience losses due to two major factors. Losses that the atom-cavity system experiences are due to atomic decay γ and cavity decay κ. Atomic decay γ results from the spontaneous emission rate of the atom as it transitions from $|e\rangle$ to $|g\rangle$. The atom re-emits the photon in a direction perpendicular to the optical axis of the cavity, leading to losses. The cavity loss rate κ is related to both the time spent of a photon in the cavity and the reflectivity of the mirrors and is defined as,

$$\kappa = \frac{\pi c}{2L\mathcal{F}} \tag{2.13}$$

Since mirrors do not have 100% reflectivity, each time the photon comes into 'contact' with the mirror, there is a chance that the photon gets transmitted out of the cavity instead of remaining in the cavity; the frequency of this increases as the cavity length L decreases. Hence, it is expected that for a low κ, the cavity length L is high, while high reflectivity mirrors $\rightarrow$ high cavity finesse $\mathcal{F}$ also results in low κ.

In the regime of $g \ll (\kappa, \gamma)$, the photons are lost from the system faster than the characteristic transition time; hence, this is the weak coupling regime. However,

if $g \gg (\kappa, \gamma)$, the system would be operating in the strong coupling regime where CQED actually holds.

In the next chapter, we will discuss more about other forms of losses in the form of noise.

Chapter 3

Noise of an optical cavity

Noise in an optical cavity affects its transmission, causing some detuning around the cavity's resonant frequency.

The noise of an optical cavity is attributed to fluctuations in cavity length. Some significant sources of noise for our optical cavity include short-term noise, such as vibration due to external surroundings, and long-term noise, such as piezoelectric creep and thermal noise. In this chapter, we will discuss the sources of noise mentioned more and possible ways to mitigate them.

3.1 Sources of Noise

3.1.1 Vibrations

Optical setups are incredibly susceptible to vibrations from the surroundings; hence, most, if not all, optical setups utilise an optical table to isolate the setup from vibrational noise from the ground. Acoustic noise affects the optical instruments by causing internal vibrations[10] and cannot be removed using an optical table. This could cause resonance within the cavity if the acoustic noise matches the natural frequency. One way to minimise the effects of acoustic noise would be to increase the natural frequency of the system. Our cavity can be simplified into a mass-spring system with m_1 and m_2 representing the mass of the brackets, k as the spring constant and x_1 and x_2 representing the small distance travelled by the brackets.

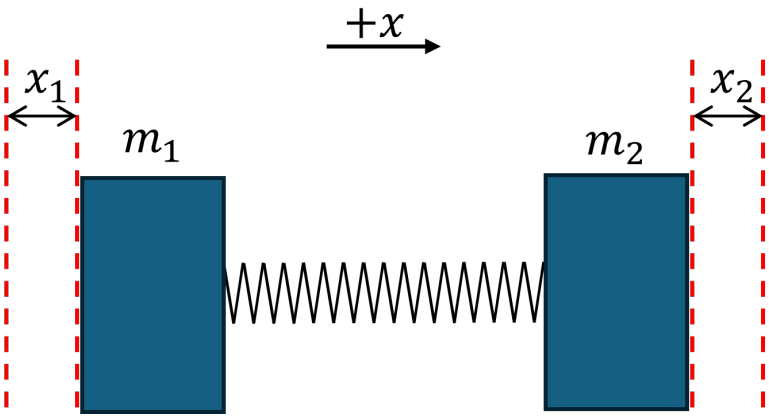

Figure 3.1: 2-mass-spring system

Considering the equations of motion of this system:

$$\begin{aligned} m_1\ddot{x}_1 &= -k\,(x_1 - x_2) \\ m_2\ddot{x}_2 &= -k\,(-x_1 + x_2) \end{aligned} \tag{3.1}$$

Assuming that the system undergoes harmonic motion during resonance, we have $x_1 = A_1 e^{i\omega t}$ and $x_2 = A_2 e^{i\omega t}$ as solutions. Substituting them into Equation 3.1,

$$\begin{aligned} m_1\omega^2 &= k\left(1 - \frac{A_2}{A_1}\right) \\ m_2\omega^2 &= k\left(1 - \frac{A_1}{A_2}\right) \end{aligned} \tag{3.2}$$

Assume that the two masses are the same (i.e. $m_1 = m_2$), $A_1 = \pm A_2$, depending on whether the masses move in-phase or out-of-phase of each other. When $A_1 = A_2$ (in-phase),

$$\begin{aligned} m\omega^2 &= k\ (0) \\ \omega^2 &= 0 \Rightarrow f = 0 \end{aligned} \tag{3.3}$$

where f is the natural frequency of the system. This suggests that the restoring force does not affect the system after the two masses move off in unison. This would not be possible in our cavity system.

When $A_1 = -A_2$ (out-of-phase),

$$\begin{aligned} m\omega^2 &= k\ (1+1) \\ \omega^2 &= \frac{2k}{m} \Rightarrow f = \frac{1}{2\pi}\sqrt{\frac{2k}{m}} \end{aligned} \tag{3.4}$$

This suggests that for a 2-mass and spring system, f would increase as k increases. Adding more springs in parallel would also facilitate an increase in the effective spring constant k_{eff} in the system. This helps prevent the system from resonating while attempting to operate a closed-loop control feedback at lower frequencies. This can also help raise the frequency ceiling within which the feedback loop operates.

3.1.2 Thermal Noise

Thermal noise present in an optical cavity is a result of Brownian motion and is very prominent in interferometric laser gravitational wave antennas, which make use of large mirrors over 400km apart and with long integration times, allowing for thermal noise to build up. This is also becoming a significant noise present in high-finesse cavities. However, thermal noise cannot be fully eliminated and is considered to be the noise floor for optical systems[11, 12]. Some ways to mitigate thermal noise would be to utilise mirror materials like fused silica, cool down the mirrors or use thicker mirrors [13].

3.1.3 Piezoelectric Creep

Piezoelectric actuators are often used in micropositioning due to their fast frequency response and high resolution. However, they experience the creep phenomenon, which is a drift in the actuator's displacement for a constant applied electric field [14]. Creep occurs as the piezo responds to a sudden change in applied voltage. The piezo will have an initial response to the voltage and will slowly drift over the next few hours. This is because the domain of dipoles present in the piezoelectric material gradually shifts with time, leading to a gradual change in length over time. The creep can be modelled using the following equation:

$$L(t) = L_O \left[1 + \gamma log_{10}\left(\frac{t}{0.1}\right)\right] \tag{3.5}$$

where $L(t)$ is the actuator's displacement for any fixed input voltage, L_O is the displacement of 0.1s after applying the input voltage, and γ is a creep factor that determines the rate of the logarithm.

Piezoelectric creep is a significant source of error as we would like to keep the cavity static at the resonant length for strong atom-light interaction. Fortunately, the piezoelectric creep can either be reduced or eliminated using capacitors in series with

the actuator[15], or using a closed-loop control system [16]. A common technique used in closed-loop controls for cavities is the Pound-Drever-Hall (PDH) technique. We will discuss more about how the technique works and how we can use it for noise measurement.

3.2 Pound-Drever-Hall Technique

One of the most common approaches to stabilise a laser to a stable cavity is the Pound-Drever-Hall (PDH) technique. It uses a frequency modulated beam sent into the cavity, collecting the reflected beam off the cavity in a photodiode, and mixing it with the modulation signal to obtain an error signal from the cavity.

3.2.1 Error Signal

An error signal can be seen as the difference between the desired point of the process variable, the lowest voltage readout from the photodiode (i.e. low reflectance or high transmission), and the actual point. This signal will be sent back into the system to correct it towards the desired point. However, we are only able to glean the magnitude of the detuning but not the direction of the detuning due to the symmetry about the signal trough. We would not be able to determine between positive and negative detuning. By taking the derivative of the signal, it gives us an asymmetric signal curve around the desired point.

We are then able to differentiate between positive and negative detuning. A good error signal should also have a steep slope around the desired point. This results in a higher signal-to-noise ratio, as a small detuning leads to a large signal.

3.2.2 How it works

The PDH technique can be used to lock both a laser to a stable cavity or a cavity to a stable laser, however, the setup would be slightly different between the two.

A frequency modulated beam is achieved using an electro-optic modulator (EOM). It uses two parallel plate capacitors to create an electric field to alter the refractive index of the non-linear crystal in between the plates. Additionally, we can apply an AC voltage to the capacitors to generate a fast-oscillating electric field, which causes rapid changes to the refractive index, imparting a phase modulation to the beam.

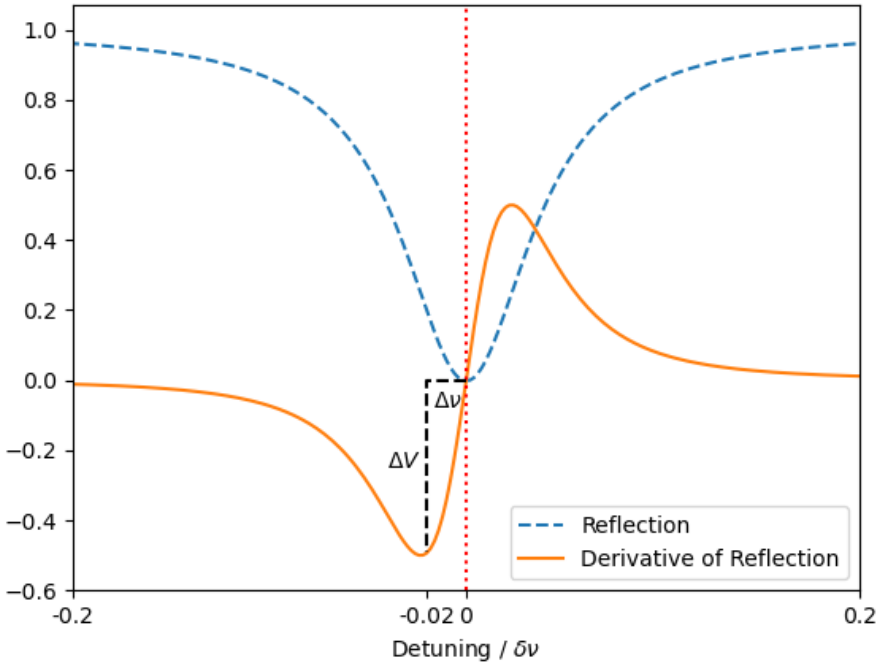

Figure 3.2: Plot of cavity reflection and its derivative. A steeper slope results in more correction ΔV for small $\Delta\nu$.

We start by considering an input beam of frequency ω,

$$E_i = E_0 e^{i\omega t} \tag{3.6}$$

We now apply a sinusoidally varying potential voltage to the EOM with frequency ω_0 and small amplitude α. Since α is small, we will keep the 1st order terms of the Taylor expansion,

$$\begin{aligned} E &= E_0 e^{i\omega t + \alpha \ sin \ \omega_0 t} \\ &\approx E_0 e^{i\omega t}\left[1 + \frac{\alpha}{2}\left(e^{i\omega_0 t} + e^{-i\omega_0 t}\right)\right] \end{aligned} \tag{3.7}$$

We can see that after modulation, the output beam contains 3 frequencies: the initial frequency ω, and 2 additional frequencies $\omega \pm \omega_0$, which are referred to as the sideband frequencies. These can be seen as 3 beams of different frequencies and form error signals that are equidistant in timescale to each other.

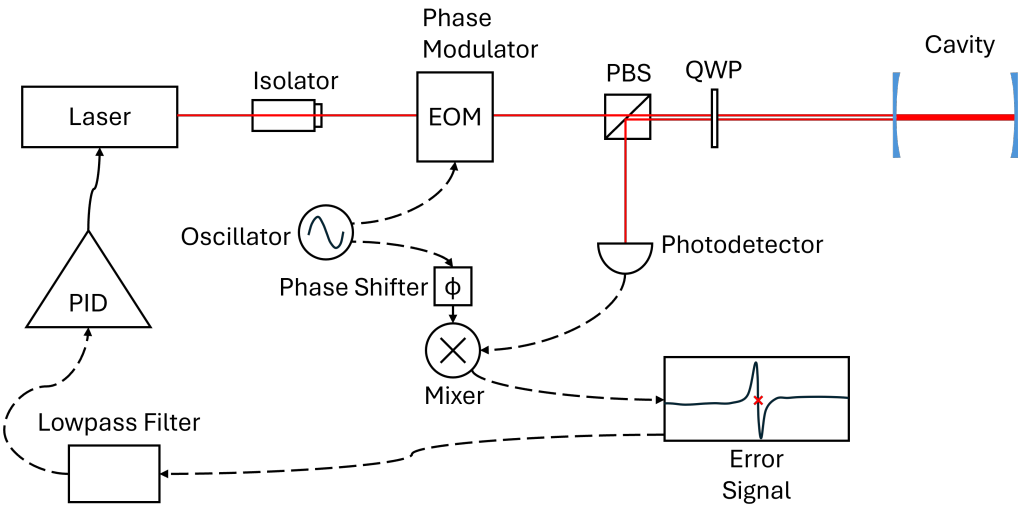

Figure 3.3: Setup using PDH to lock laser to cavity.

3.3 Mechanical Noise Extraction

By locking the laser to a stable source, such as an atomic transition, we are able to transfer the stability of the atomic transition, in this case, the ^{87}Rb D_2 line [17], to the laser. By introducing a slow lock to the control loop locked onto the error signal of the laser, we can remove the effect of piezoelectric creep on the laser. By doing so, the noise inherent to the laser can be extracted by measuring the voltage readout over a 10 s integration time period. The same can be done for the cavity while it is being locked to the laser. The noise measurement will be in terms of voltage fluctuations instead of actual length measurements, which can be later converted into its frequency and length counterparts.

3.3.1 Voltage Conversion

One way to convert the readout measurements to from voltage frequency would be to use known frequency rulers such as the sideband frequencies if the cavity linewidth, $\delta\nu$ is much less than the modulation frequency ω_0. This is considered the fast modulation regime. By driving the laser with a periodic ramp signal, we are able to extract the conversion factor from time scale to frequency due to the signal's linearity.

$$\Delta f = \omega_0 \cdot \frac{dV}{dt} \cdot \Delta t_0 \tag{3.8}$$

where $\frac{dV}{dt}$ is the slope of the error signal around the zero-crossing point and Δt_0 is the time scale difference between the zero crossing point to one of the ω_0 sidebands. However, if $\delta\nu \simeq \omega_0$, sidebands would not be visible in the error signal, and we will not be able to use the above method to convert the results. In the slow modulation regime, we would require other frequency rulers, such as the known transition probability between the ^{87} Rb D_2 of 133.3 GHz. From here, we are able to convert from frequency fluctuations to length fluctuations in the cavity.

3.3.2 Frequency Conversion

Frequency fluctuations are a good enough indicator of noise, however, the aim of this thesis is to investigate the effects of springs on the stability of a near-concentric cavity. Hence, the conversion from frequency noise to length fluctuation is necessary to paint a more intuitive picture of how springs affect the stability of the cavity. We use Equation 2.7 and Equation 2.8 to find the conversion factor from frequency to length,

$$\begin{aligned} \frac{\Delta L}{L_{fsr}} &= \frac{\Delta\nu}{\nu_{fsr}} \\ \Delta L &= \frac{\lambda L}{c}\Delta\nu \end{aligned} \tag{3.9}$$

3.3.3 Stability requirement

Based on previous works[9], a stability requirement, ξ was implemented as a result to aim for. ξ is defined to be the noise limit factor for our near-concentric cavities, which normalises the ratio of the frequency fluctuation $\Delta\nu$ due to mechanical noise to the cavity linewidth, $\delta\nu$. We can use Equation 3.9 to convert ξ to depend on length fluctuation, ΔL instead.

$$\xi = \frac{\Delta\nu}{\delta\nu} = \frac{2\Delta L}{\lambda}\mathcal{F} \tag{3.10}$$

The noise limit factor, ξ can be seen as a measure of passive stability. A noise limit factor, ξ of 1 indicates that the cavity fluctuation is equal to its linewidth. Previously, a $\xi \approx 0.05$ was attained, and we hope to be able to achieve a ξ value below that. One of the ways that we could reduce ξ would be through the use

of springs. We will discuss more regarding passive noise stabilisation in the next chapter.

Chapter 4

Springs

The third design uses MISUMI tension springs made of 304 stainless steel wires with a wire diameter of 0.5 mm and a spring constant of 1.2 N mm^{-1}. They also had a rest length of 12.5 mm. 304 stainless steel was used as it is suitable for use in an ultrahigh vacuum setup[18], with a low outgassing rate and stability in high temperatures, and it is a commonly-used material. One of the issues discovered by the previous team was that the springs experienced very weak ferromagnetic properties even though they were austenite. This caused the springs to be affected by the magnetic fields present. When the field is switched off, the springs will start to oscillate, which causes the cavity length to fluctuate uncontrollably. The ferromagnetic properties of austenite stainless steel are commonly attributed to small amounts of martensite contained within [19].

Hence, one of the solutions that we propose to solve this issue with ferromagnetism is to use materials that do not exhibit such properties in any of their phases. One such candidate is titanium, namely, Grade V titanium alloy, which usually contains 3.5% vanadium and 5.5% aluminium by weight. However, titanium tension springs with small spring diameters are not commercially available, hence, we also propose to make the springs in-house.

4.1 Making Springs

Spring-making is an intricate art that requires the use of specialised tools and equipment to yield consistent products with repeatable results. We have a lack of such machinery, hence, we utilise titanium wires, a hand drill, and a drill bit with a diameter of 1.5 mm as the arbour (a). We first threaded the wire along the grooves

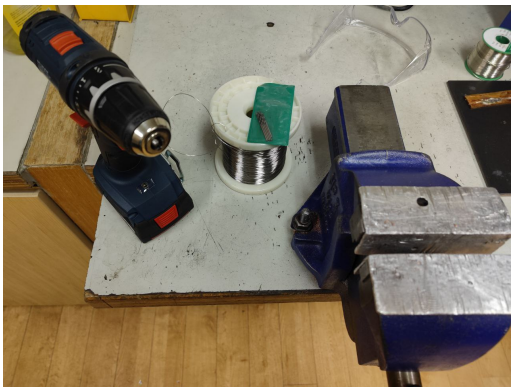

(a) Equipment needed to make springs

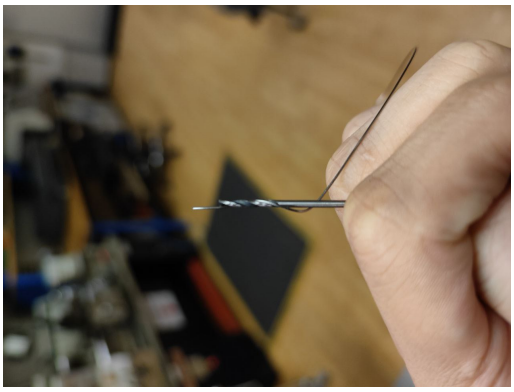

(b) Coiling wire around drill bit

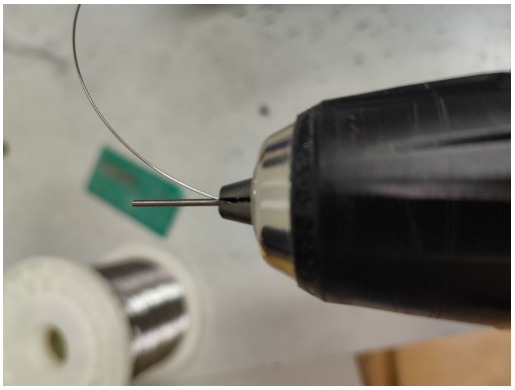

(c) Bend wire slightly to maximise length

(d) Maintain tension while coiling

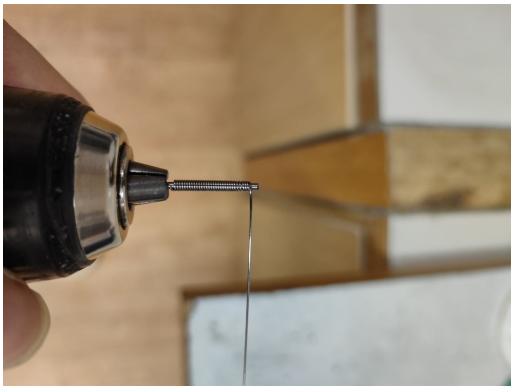

(e) Coil spring until length of arbour (kinks in spring due to uneven tension)

(f) Cut spring down to length and to avoid kinks

Figure 4.1: Steps (a-f) to make springs

of the drill bit tip (b) before placing it tip-first into the mouth of the hand drill (c). We will then coil the wire slowly along the drill bit while maintaining constant tension (d) until the wire wraps along the entire arbour length (e). Finally, we will cut the spring to the desired length (f). As the constant applied tension is removed,

the spring relaxes and expands slightly in diameter. Hence, we use an arbour of 1.5 mm to coil the springs to an inner diameter of around 2 mm. Being able to make our own springs means that we have the freedom to modify the spring parameters, which allows us to explore how the different parameters would lead to greater cavity stability.

4.2 Spring Constant

The spring constant is the central parameter to vary while exploring how changing springs could work as effective passive noise reduction. The spring constant, k is given in [20].

$$k \approx \frac{Gd^4}{8ND^3} \tag{4.1}$$

where G is the shear modulus, d is the wire diameter, N is the number of active loops in the spring, and D is the spring diameter. The equation can be further simplified for our setup as we use the same inner diameter. Hence,

$$k = \frac{Gd^4}{8N(D_I + d)^3} \tag{4.2}$$

With this equation in mind, we proceeded with creating springs using titanium while experimenting with different d and N values. We first experimented by keeping all other parameters, except G, k, and D_I, constant with respect to the commercial MISUMI springs used in the previous setup. Hence, we made titanium springs with the following parameters:

	d/mm	D_I/mm	N	Length/mm	k /N mm^{-1}
1	0.5	1.68(1)	27	13.5	0.90(1)
MISUMI	0.5	2	27	13.5	1.2

Table 4.1: Comparing Spring 1 and MISUMI springs

The spring constants k were measured using a digital micrometer and a digital force gauge in a setup as shown below.

Spring 1 was made with similar parameters with the MISUMI springs and it is evident that the type of material used affects spring constant, k. Grade V titanium has a shear modulus, G_{Ti} of 40 - 45 GPa, while 304 stainless steel has a larger

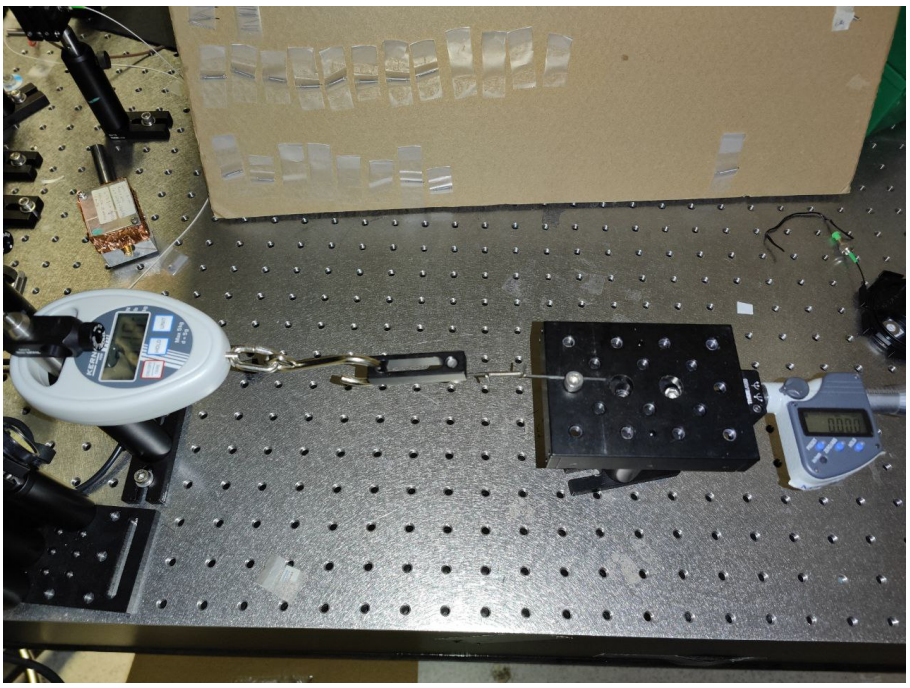

Figure 4.2: Micrometer and force gauge for spring constant, k measurement.

shear modulus, G_{304} of 74 - 81 GPa. Additionally, the inner diameter, D_I is also smaller than the MISUMI springs, which increases k. Using Equation 4.2 and the aforementioned parameter differences, we expect spring 1 to have a spring constant, k 0.75 times that of the MISUMI springs, which is also what we observe from measurements.

To achieve k of similar values, we decided between reducing N or increasing d. Reducing N is very straightforward, it can be easily done by cutting the spring loops out. However, reducing N reduces the rest length of the spring, l, causing it to extend more when placed into the cavity and increasing the spring force. One worry is that the springs would plastically deform after long periods of extension under high stress. Hence, we decided to instead increase d to obtain a higher spring constant k. From Figure 4.3, we can see the exponential relationship between spring constant k and wire diameter d. Below are the parameters for spring 2,

	d/mm	D_I/mm	N	Length/mm	k /N mm^{-1}
2	0.6	1.68(1)	27	16.2	1.90(9)

Table 4.2: Parameters for spring 2

However, we noticed that after assembling the cavity with spring 2, the two

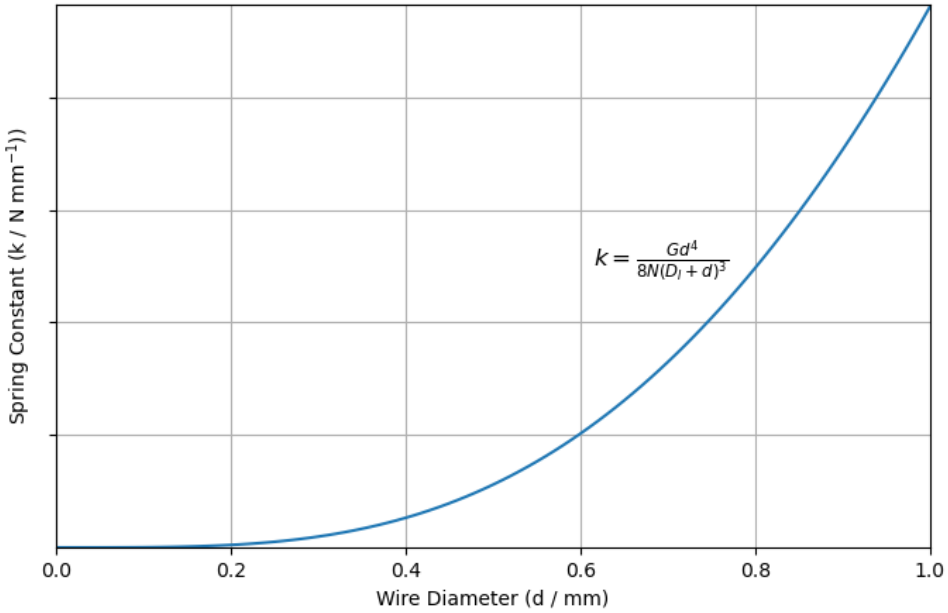

Figure 4.3: Relationship between spring constant, k and wire diameter, d, while keeping N, D_I and G constant

brackets of the cavity were more prone to translational and rotational movement compared to the previous iteration with spring 1. This was an interesting result as the newer cavity has a higher propensity for unstable motion compared to the previous one, even though the springs have a higher spring constant, k. This suggests that our previous hypothesis that k would increase stability for our cavity setup was incorrect and that k should only affect the natural frequency of the system. One possible explanation for this discrepancy would be the spring force.

4.3 Spring Force

The cavity system that we are using for our experiments has a restriction that was not considered in the previous 2-mass spring system. The length of the spring, when it is extended within the cavity structure, is fixed to 18 mm. Notably, the piezoelectric stack actuators have a nominal range of around 15 μm, causing a 0.08% change in the spring length when fully extended, so we will not consider the effects of the actuators on the springs. Using Hooke's Law and considering the final length

of the spring,

$$\begin{aligned} F &= k \cdot (L_C - l) \\ F &= k \cdot (L_C - N \cdot d) \end{aligned} \tag{4.3}$$

where $L_C = 18$ mm is the length of the spring extended in the cavity and l is the rest length of the spring.

The spring force for spring 1, F_1 is calculated to be 4.05 N, while the spring force for spring 2, F_2 is calculated to be 3.42 N. The spring force calculated only takes into consideration a single spring, while there are 4 springs in the cavity design, which results in a more noticeable difference in total force of 2.52 N. We suspect this to be the reason behind the difference in the stability of the cavity. To find out the dependence of F on d, we substitute Equation 4.2 into the spring force equation Equation 4.3,

$$F = \frac{Gd^4}{8N\left(D_I + d\right)^3} \cdot (L_C - N \cdot d) \tag{4.4}$$

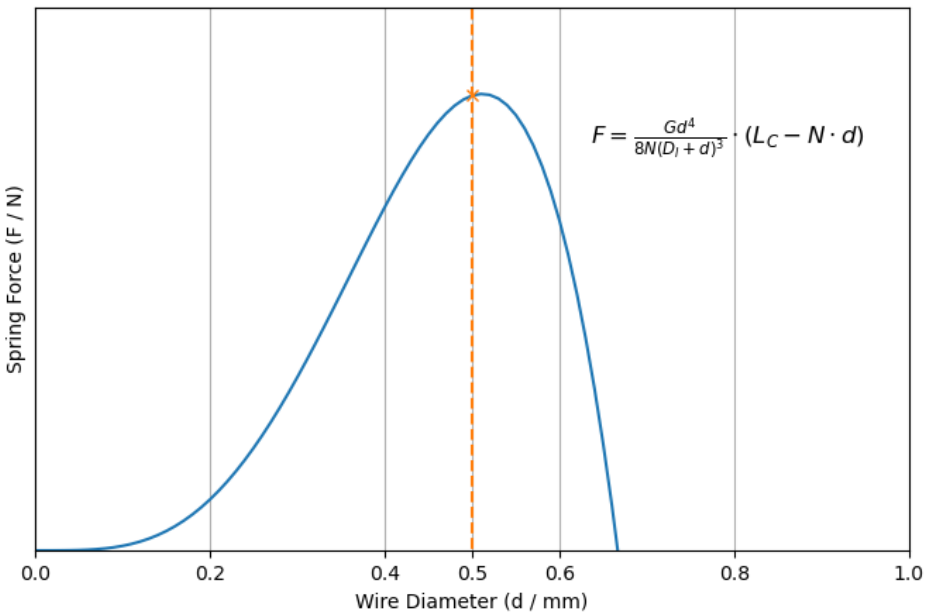

Figure 4.4: Relationship between spring force, F and wire diameter, d, while keeping 4, D_I and G constant. Peak force at around $d = 0.5$ mm

One expects a high k value to result in a higher spring force, which would lead to higher cavity stability. However, since the length of the spring is fixed to be

around 18 mm when extended within the cavity structure, this limits how much the spring can stretch. As shown in Figure 4.4, the spring force peaks out at around 0.5 mm, and further increasing d yields a lower spring force, as we observed. Therefore, increasing d alone is not sufficient to effectively increase the spring force to better stabilise the cavity. Hence, to increase the spring force, we would have to decrease N as well. Previously, decreasing N ran a risk of plastic deformation, but by increasing d, it increases the cross-sectional area of the spring, which in turn lowers the stress experienced by the spring.

Since the MISUMI springs have a spring force of 5.4 N when placed in the cavity, we aim for the next iteration of springs to have a spring force higher than that. We achieve this by decreasing N while increasing d. We continue to use titanium wires of $d = 0.6$ mm to make spring 3, with $N = 25$ loops instead of 27.

	d/mm	D_I/mm	N	Length/mm	k /N mm^{-1}
No. 3	0.6	1.68(1)	25	15	2.124(6)

Table 4.3: Parameters for spring 3

The spring force for the 3rd iteration of springs is calculated to be 6.37 N, and the total spring force is 3.88 N more than the MISUMI setup. Using spring 3, the cavity is stiffer and less prone to movement as compared to when spring 1 was used. Hence, spring 3 appears to be a good candidate to test the effects of higher F and k.

Chapter 5

Experimental Setup and Results

We first create a prototype in a near-planar configuration to test our hypothesis. A near-planar configuration is much easier to assemble and serves as a good estimate of the effect of springs on the stability of a near-concentric cavity. We plan to move on to a near-concentric configuration if desirable results are produced.

5.1 Near-Planar Cavity

Instead of working directly with a near-concentric cavity, we first work with a near-planar cavity to characterise the effects of the springs on noise reduction.

We will be working with spherical mirrors of 99.9% reflectivity. The mirrors have a radius of curvature of 100 mm, while the length of the cavity is around 11 mm, which puts the cavity in a near-planar configuration. Using the cavity design shown in Figure 1.5, the cavity parameters were experimentally obtained as such: There

Variables	Theoretical	Measured
ν_{fsr}	13636 MHz	14895(55) MHz
Linewidth	4MHz	9(1)MHz
Finesse	3140	1660

Table 5.1: Cavity Parameters for Near-Planar Cavity

are discrepancies between the theoretical and measured values. Firstly, for ν_{fsr}, the theoretical value was calculated with a cavity length of 11 mm; however, the actual cavity length could have been shorter, around 10.07(3) mm, since the mirrors were glued by eye. Secondly, for both linewidth and finesse, one explanation would be

the mirror reflectivity being slightly lower than expected, at 99.8% instead of 99.9% due to dirt or slight imperfections on the mirror surface.

5.1.1 Springs

In general, as we construct each spring by hand, there may be issues regarding the consistency of the springs; kinks within the spring may form because of inconsistent applied tension while coiling. As such, we choose 4 springs with similar spring constants from every batch of springs made for springs 1,2, and 3. Below is a table with the measured spring constants, k,

No.	Quantity made	k / N mm^{-1}	k_4/N mm^{-1}
1	12	0.91(4)	0.90(1)
2	16	1.9(1)	1.90(9)
3	12	2.13(5)	2.124(6)

Table 5.2: Average of all spring constants from all springs

Spring 1 resulted in an unstable cavity, and we were not able to lock onto the error signal. Hence, we were not able to obtain any noise measurements. Spring 2

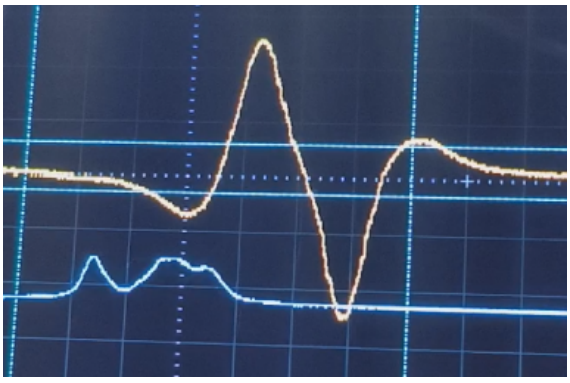

Figure 5.1: Blue line at the bottom corresponds to the transmission graph of the cavity with spring 1. A Gaussian curve is expected if the cavity is stable at the resonance frequency.

was not experimented with as the cavity itself was prone to movement and was not stiff enough.

Spring 3 resulted in a stable enough cavity for a lockable error signal to be found, and we are able to make use of the PDH technique to measure the cavity noise

5.1.2 Mechanical Noise

The mechanical noise of the near-planar cavity is measured using the PDH technique, locking the laser to the cavity and reading the voltage fluctuations in the error signal. We then use the conversion factors from Equation 3.8 and Equation 3.9 to convert it into frequency noise and length fluctuation. There is an overlap between the laser and cavity noise spectral densities; the noise peaks at 45 Hz and 600 Hz are also visible for both laser and noise spectral densities. This suggests that the noise from the cavity can be partly attributed to the laser.

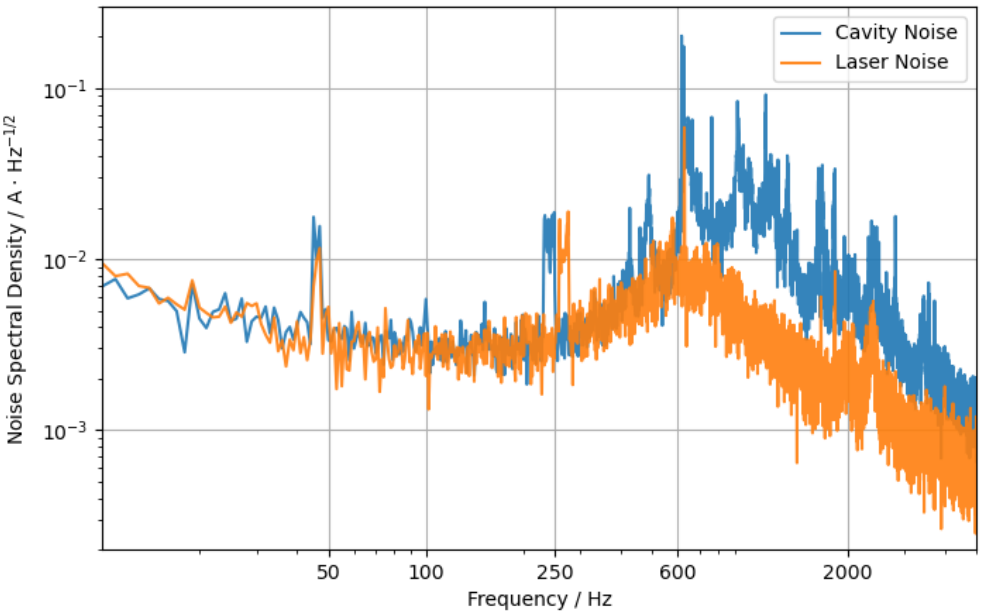

Figure 5.2: Noise Spectral Density graph of both laser and cavity in logarithmic scale

Averaged over three measurements, the laser frequency noise was measured to be 0.206(7) MHz, while the cavity frequency noise was measured to be 0.33(1) MHz. Converted to length fluctuations, it results in a near-planar cavity noise of 0.092(3) Å. We can also expect the near-concentric cavity to have length fluctuations along the same order of magnitude. Comparing this result to previous works, they had a passive length fluctuation of 0.36(2) Å. This results in a ξ value of 0.039(1), which is below the $\xi = 5\%$ of the previous iteration.

Compared to previous works, this result provides a significant improvement of 4 times in terms of length fluctuation, suggesting that further in-depth exploration is necessary, especially using a near-concentric configuration instead. We expect to see lower ξ values from a near-concentric cavity like from previous works, as the finesse value is 627 compared to our measured cavity finesse of 1660.

5.1.3 Resonance

To investigate the effects of increasing the spring constant, k on the natural frequency, f of the cavity, we used a network analyzer (Agilent E5061b 3GHz Network Analyzer) to characterise the resonant frequency of the cavity. The network analyzer generates an AC current that sweeps between the selected frequency range. This signal is then fed into one of the piezoelectric actuators, introducing a driving frequency to the system. The cavity error signal is then collected.

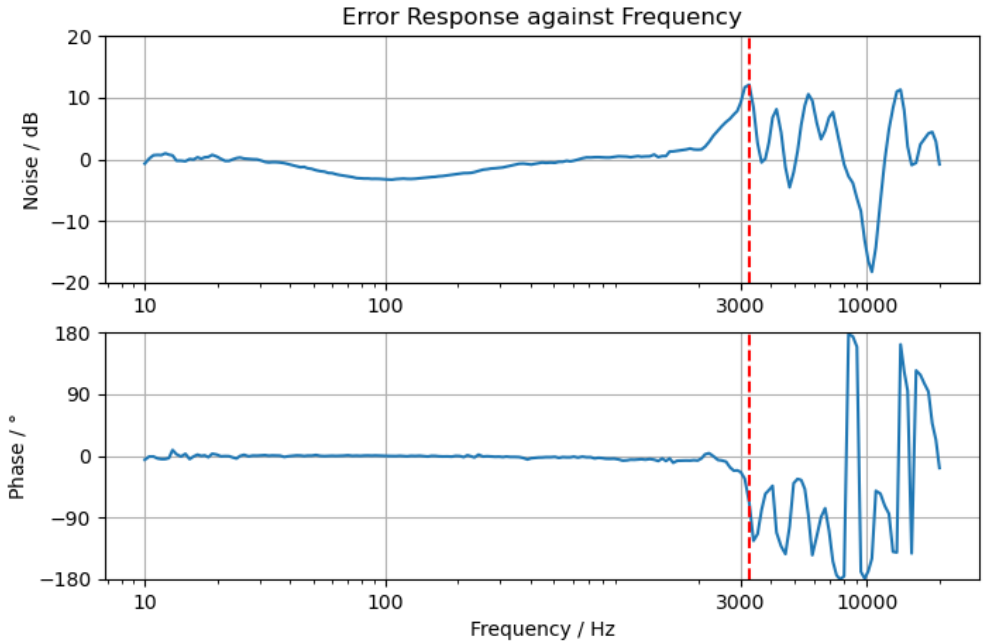

Figure 5.3: Plot of mechanical response due to a driving piezoelectric actuator. The red dotted line marks the first resonant mode.

The first resonant mode is marked at 3241 Hz by the noise peak and the phase shift of 90°. This is an increase in natural frequency, f, compared to past iterations of 2750 Hz, and it suggests that the increase spring constant k, does indeed lead to

a higher f. This result agrees with Equation 3.4 and would entail that a closed-loop system could operate at higher frequencies, up to 3000 Hz (i.e. increased control bandwidth).

Chapter 6

Conclusion and Future Work

6.1 Conclusion

In the previous iteration of our near-concentric cavity, a complete redesign of the cavity introduced fewer moving parts, reducing its mechanical complexity. However, it was found that the stainless steel springs were slightly ferromagnetic, which caused major length fluctuations when taken out of a magnetic field. In order to not be affected by the magnetic field, we considered using a new material to be used for the springs of the cavity. One of the properties that we looked for in a material was being non-ferromagnetic. The stainless steel used for the MISUMI springs was supposed to be austenite, but it was discovered that there could be trace amounts of ferromagnetic elements within.

Hence, for a complete shift away from steel-based springs, we decided to explore using titanium to make our own springs. Making our own springs meant that we could tinker around with the parameters, such as wire diameter and number of loops, to explore the role of each parameter and how it affects the overall cavity stability. One of the more interesting results was that increasing the spring constant did not necessarily lead to an increase in the spring force as well. This was due to the design of the cavity limiting the spring to extend to 18 mm in length. As expected, the increase in spring constant k led to an increase in the natural frequency of the cavity. This would allow for closed-loop controls with high control bandwidth.

The spring force played a dominant role in the passive stability of the cavity. The stiffness from the springs lowered passive length fluctuations to 0.092(3) Å, which was a great improvement over 0.36(2)Å.

6.2 Future work

One of the things that would be obvious would be to transfer the four spring 3s to an optical with a near-concentric configuration. A need for lower $\mathcal{F}$ mirrors means that a near-concentric cavity could operate at extremely low ξ values of 0.015.

Another thing that could be done would be to explore methods to mitigate the effect of thermal noise, by forms of cooling or the use of different mirror materials.

Bibliography

[1] W.-K. Lee, C. Y. Park, M.-S. Heo, H. Kim, D.-H. Yu, G.-W. Truong, and G. D. Cole, "Ultrastable laser system using room-temperature optical cavity with 4.8×1017 thermal noise limit", in *2019 Joint Conference of the IEEE International Frequency Control Symposium and European Frequency and Time Forum (EFTF/IFC)*, 2019, pp. 1–2.

[2] T. Schneemann, K. Schmieden, and M. Schott, "Search for gravitational waves using a network of rf cavities", *Nuclear Instruments and Methods in Physics Research Section A: Accelerators, Spectrometers, Detectors and Associated Equipment*, vol. 1068, p. 169 721, 2024, ISSN: 0168-9002.

[3] M. Xiong, Q. Liu, X. Wang, S. Zhou, B. Zhou, and Z. Bu, "Mobile optical communications using second harmonic of intra-cavity laser", *IEEE Transactions on Wireless Communications*, vol. 21, no. 5, pp. 3222–3231, 2022.

[4] A. Reiserer and G. Rempe, "Cavity-based quantum networks with single atoms and optical photons", *Rev. Mod. Phys.*, vol. 87, pp. 1379–1418, 4 Dec. 2015.

[5] C. A. Potts, A. Melnyk, H. Ramp, M. H. Bitarafan, D. Vick, L. J. LeBlanc, J. P. Davis, and R. G. DeCorby, "Tunable open-access microcavities for on-chip cavity quantum electrodynamics", *Applied Physics Letters*, vol. 108, no. 4, p. 041 103, Jan. 2016, ISSN: 0003-6951.

[6] L. Gan and Z. Li, "Photonic crystal cavities and integrated optical devices", *Science China Physics, Mechanics & Astronomy*, vol. 58, no. 11, Oct. 2015, ISSN: 1869-1927.

[7] C. H. Nguyen, A. N. Utama, N. Lewty, K. Durak, G. Maslennikov, S. Straupe, M. Steiner, and C. Kurtsiefer, "Single atoms coupled to a near-concentric cavity", *Phys. Rev. A*, vol. 96, p. 031 802, 3 Sep. 2017.

[8] C. H. Nguyen, A. N. Utama, N. Lewty, and C. Kurtsiefer, "Operating a near-concentric cavity at the last stable resonance", *Phys. Rev. A*, vol. 98, p. 063 833, 6 Dec. 2018.

[9] F. Adam, W. X. Chiew, A. N. Utama, and C. Kurtsiefer, "Low noise near-concentric optical cavity design", *Review of Scientific Instruments*, vol. 95, no. 4, p. 043 102, Apr. 2024, ISSN: 0034-6748.

[10] M. Gendreau, "Specification of the effects of acoustic noise on optical tools", *Noise Notes*, vol. 2, pp. 33–40, Jul. 2003.

[11] K. Numata, A. Kemery, and J. Camp, "Thermal-noise limit in the frequency stabilization of lasers with rigid cavities", *Phys. Rev. Lett.*, vol. 93, p. 250 602, 25 Dec. 2004.

[12] S. A. Webster, M. Oxborrow, S. Pugla, J. Millo, and P. Gill, "Thermal-noise-limited optical cavity", *Phys. Rev. A*, vol. 77, p. 033 847, 3 Mar. 2008.

[13] T. Kessler, T. Legero, and U. Sterr, "Thermal noise in optical cavities revisited", *J. Opt. Soc. Am. B*, vol. 29, no. 1, pp. 178–184, Jan. 2012.

[14] H. Jung and D.-G. Gweon, "Creep characteristics of piezoelectric actuators", *Review of Scientific Instruments*, vol. 71, pp. 1896–1900, Apr. 2000.

[15] H. Kaizuka and B. Siu, "A simple way to reduce hysteresis and creep when using piezoelectric actuators", *Japanese Journal of Applied Physics*, vol. 27, no. 5A, p. L773, May 1988.

[16] E. D. Black, "An introduction to pound–drever–hall laser frequency stabilization", *American Journal of Physics*, vol. 69, no. 1, pp. 79–87, Jan. 2001, ISSN: 0002-9505.

[17] Z. Gao, Z. Ge, T. Shi, C. Zhu, X. Qin, and J. Chen, "A faraday laser locked to 87rb d2 line", *Optics Communications*, vol. 565, p. 130 677, 2024, ISSN: 0030-4018.

[18] S. Mukherjee, P. Panchal, J. S. Mishra, R. Gangradey, P. Nayak, and V. Gupta, "Hydrogen outgassing and permeation in stainless steel and its reduction for uhv applications", *Materials Today: Proceedings*, vol. 44, pp. 968–974, 2021, International Conference on Materials, Processing & Characterization, ISSN: 2214-7853.

[19] A. Das, "Magnetic properties of cyclically deformed austenite", *Journal of Magnetism and Magnetic Materials*, vol. 361, pp. 232–242, 2014, ISSN: 0304-8853.

[20] R. G. Budynas and J. K. Nisbett, "Shigley's Mechanical Engineering Design", McGraw-Hill Education, 2015, p. 512.